Memoirs of the Faculty of Engineering, Nagoya University
Vol. 32, No. 1. (1980) — Research Report —

EFFECT OF SURFACE LAYER ETCHING AND ION-DOSAGE ON BUBBLE STATE TRANSITION IN ION-IMPLANTED GARNET FILMS

SHIGERU SHIOMI and SUSUMU UCHIYAMA

Department of Electrical Engineering

(Received May 27, 1980)

Abstract

The effect of the ion-implanted surface layer on the relationship between the bubble deflection angle θ and the in-plane field H_{ip} is investigated. The samples used are either etched a part of the surface layer implanted Ne^+ ions of $100keV$ to a dosage of $7\times10^{13}cm^{-2}$ or implanted to various dosages. In the samples implanted to a dosage of $7\times10^{13}cm^{-2}$, it is found that the effective layer determining the wall structure of the underlying bubble exists in the region between 500 and 800 $\mathring{A}$ deep from the surface. In the sample implanted to as high dosage as $10^{15}cm^{-2}$, θ varies with increasing and then dcereasing H_{ip} gradually rather than abruptly as generally seen. These results are interpreted based on the relevant works on the magnetic properties of the ion-implanted layer and the bubble state transitions.

1. Introduction

Ion-implantation is now widely used for the hard bubble suppression[1] and for the control of bubble states[2]. It is also an essential technique for the bubble lattice devices[3] and contiguous disk devices[4~6], which are considered promising to achieve higher density bubble devices than the field-access ones now in use.

Therefore, a lot of works have been carried out to make clear the effect of ion-implantation. The main results obtained so far are as follows. Ion-implantation produces a surface layer with planar magnetization[7], in which closure domains associating with the underlying bubbles are observed[8]. Hard bubbles are completely suppressed if the strain-induced magnetic anisotropy K_s exceeds the as-grown uniaxial anisotropy K_u[9]. The profile of the implantation-induced damage was studied qualitatively[10] and quantitatively[11]. Under a rotating in-plane field, the closure domain as well as the bubble collapse field exhibits a three-fold symmetry[12].

Another important finding is that the kind of bubble wall structure which can stably exist in ion-implanted films is quite limited: only $S=1$ at zero in-plane field, $H_{ip}=0$, and $S=0$ at sufficiently large value of H_{ip}[2]. Here, the bubble winding number S was calculated from the relation[13],

$$S=(\gamma d \Delta H/8V)\sin\theta, \tag{1}$$

where θ is the bubble deflection angle between the pulsed gradient field and the direction of bubble translation with a velocity of V, γ the gyromagnetic ratio and ΔH the bias field difference across the bubble diameter d. At an intermediate value of H_{ip}, additional states corresponding to fractional S values were observed[14, 15]. Moreover, θ changes with increasing H_{ip}[16], and exhibits a *"hysteresis"* with increasing and then decreasing H_{ip}[17~19].

The object of this paper is to make clear the effect of the magnetic properties of ion-implanted surface layers on the bubble state transitions. To this end, the effects of the removal of ion-implanted surface layer and of the ion dosage on the bubble state transitions were studied by the usual bubble translation method with increasing and then decreasing H_{ip}. The properties of samples and the experimental procedures used here are described in 2. Experimental results are given in 3., and then discussed in *4. 3.* based on the previous works summarized in *4. 1.* and *4. 2.*

2. Samples and experimental procedures

The material parameters of the samples used are listed in Table I. All the samples have the same composition $(Y_{1.36}Eu_{0.20}Yb_{0.58}Ca_{0.86})(Ge_{0.86}Fe_{4.14})O_{12}$ supporting about 3 μm diameter bubbles. The samples were cut from the five different wafers A, B, C, D and E into the rectangular shape with a dimension of ~ 5 *mm*. The samples were implanted with 100 *keV* Ne^+ ions to various dosages. The dosage of the wafer A and B is 7×10^{13} cm^{-2}, which was empirically found to be adequate for the hard bubble suppression in these films. The surface layers of

Table I : Material Parameters of $(Y_{1.36}Eu_{0.20}Yb_{0.58}Ca_{0.86})(Ge_{0.86}Fe_{4.14})O_{12}$ Chips.

Sample	A_1	A_2	B_1	B_2	C_1	C_2	D	E
Film Thickness h (μm)	3.16		3.58		3.09		2.88	3.19
Stripe Width S_w (μm)	2.90		3.13		2.98		2.97	3.02
Collapse Field H_{col} (Oe)	148		143		141		134	144
Characteristic Length l (μm)	0.325		0.344		0.343		0.348	0.341
$4\pi M_s$ ($Gauss$)	265		260		263		267	273
Ion Species	Ne^+							As-Grown
Implantation Energy (keV)	100							
Implantation Dosage ($1/cm^2$)	7×10^{13}				2×10^{14}	5×10^{14}	10^{15}	
Etched-Layer Thickness ($\mathring{A}$)	—	480	—	800	—	—	—	

the samples A_2 and B_2 were etched by 480 and 800 $\mathring{A}$, respectively, to investigate the magnetic properties of the ion-implanted layer. The etched-layer thickness was measured using Tallysteps. The samples C_1, C_2 and D were implanted to dosages of 2×10^{14}, 5×10^{14} and $10^{15} cm^{-2}$, respectively, to investigate the influence of an ion dosage. The sample E is an as-grown, non-implanted film used for comparison.

The dynamic properties of bubbles were measured by the usual bubble translation method described by Vella-Coleiro and Tabor[20]. The parallel conductors were 10 μm wide and separated 80 μm center-to-center. Bubble domains were observed using a polarizing microscope. The bubble deflection angle and translation distance were measured using an eye-piece graduater and an eye-piece micrometer, respectively. The total magnification of the microscope was 400 times in any case. In order to improve the accuracy of measurement, it is desirable to increase the total bubble displacement. However, it was observed that the bubble deflection angle θ and the bubble displacement per pulse Δx were increased as the bubble domain approached conductor lines closely, probably due to the non-uniformity of the field gradient. Therefore, all the data were taken in the middle region between the parallel conductors with a width of about 10 μm.

Pulsed drive field ΔH, which is defined as the field difference across the bubble diameter, and pulse duration T were 3 Oe and 300 $nsec$, respectively. Bubble deflection angle θ was measured as a function of an in-plane field H_{ip} which was increased up to 160 Oe and then reduced to zero. The in-plane field H_{ip} was applied parallel to ∇H except the case shown in Fig. 1 (b) where H_{ip} was applied perpendicular to ∇H. The values of θ plotted in Figs. 1~7 are the average of five measurements.

3. Experimental results

The relationship between the bubble deflection angle θ and the in-plane field H_{ip} in the sample A_1 implanted to the standard dosage of 7×10^{13} Ne^+/cm^2 is shown in Fig. 1. In the case of $H_{ip}/\!/\nabla H$, θ decreases slightly with increasing H_{ip}, then it abruptly decreases to zero at $H_{ip}\simeq150Oe$ (the first transition) as shown in Fig. 1 (a). When H_{ip} is decreased from a value larger than 160 Oe, θ remains at almost zero until $H_{ip}\simeq70$ Oe where a second transition appears showing a finite θ. With further decrease of H_{ip}, θ increases gradually and finally the third transition to the initial state takes place at $H_{ip}\simeq0$. In the case of $H_{ip}\perp\nabla H$ shown in Fig. 1 (b), the θ *vs.* H_{ip} relation is almost the same as that in the case of $H_{ip}/\!/\nabla H$ shown in Fig. 1 (a). It is noted, however, that θ increases slightly as the initial increase of H_{ip} and that the values of θ during the decrease of H_{ip} after the second transition are slightly larger than those in the case of $H_{ip}/\!/\nabla H$. In the case of Fig. 1 (c), H_{ip} parallel to ∇H is first increased to a value of 160 Oe (closed circles), then decreased to 20 Oe (open circles), and again increased to 160 Oe (crosses). With the second increase of H_{ip} from 20 Oe to 160Oe, θ decreases gradually to zero without showing clear transition. The similar results were obtained in the sample B_1, which was also implanted to the standard dosage of 7×10^{13} Ne^+/cm^2. These results for the sample A_1 are quite similar to those reported by Beaulieu *et al.*[17] as will be discussed later. Therefore, we consider the sample A_1 to be the reference sample in the present study.

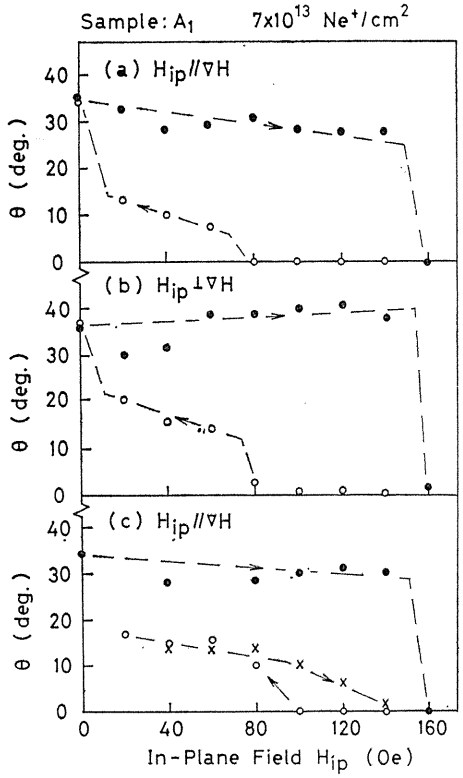

Fig. 1. The relationship between bubble deflection angle θ and in-plane field H_{ip} in the sample A_1·H_{ip}, either parallel or perpendicular to gradient field ∇H, is increased to 160 *Oe* and then decreased to zero. In (c), H_{ip} is again increased from 20 *Oe* to 160*Oe*.

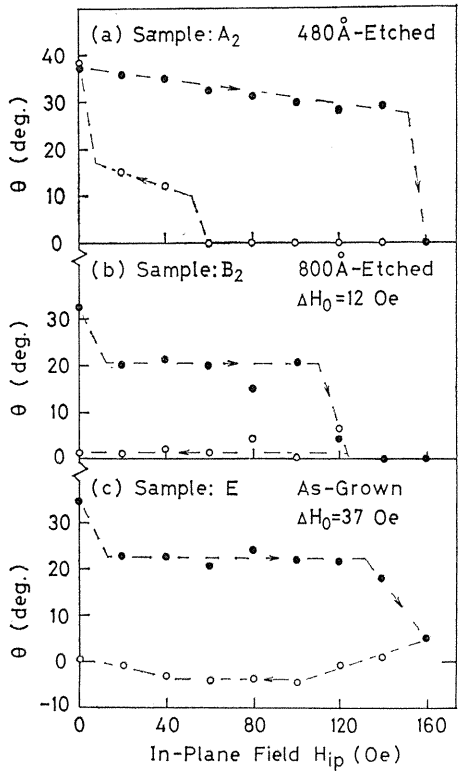

Fig. 2. The θ versus H_{ip} relation in the surface-etched samples; 480 Å (a) and 800 Å (b). The sample E in (c) is as-grown for comparison.

The effect of the removal of the ion-implanted surface layer is shown in Fig. 2. Figure 2 (a) shows the θ *vs.* H_{ip} relation in the sample A_2, the surface layer of which was implanted to the standard dosage of 7×10^{13} Ne^+/cm^2 and then etched by 480 Å. It is noted that the θ *vs.* H_{ip} relation in the sample A_2 is quite similar to that in the reference sample A_1 shown in Fig. 1 (a). Figure 2 (b) shows the results in the sample B_2, the surface of which was implanted to the standard dosage of 7×10^{13} Ne^+/cm^2 and then etched by 800 Å. It was observed in the sample B_2 that all the bubbles did not collapse in unison at a critical bias field. The scatter of the static collapse field ΔH_{col} among a lot of bubbles generated by stripe domain cutting was about 12 *Oe*. Thus, the stable bubble state at $H_{ip}=0$, which can be distinguished from the value of θ, is not unique as in adequately implanted samples. Therefore, the bubble domain which was identified to be S=1 from its deflection angle of about 33 *degrees* at $H_{ip}=0$ was selected to take the data shown in Fig. 2 (b). With increasing H_{ip}, θ initially decreases rather abruptly

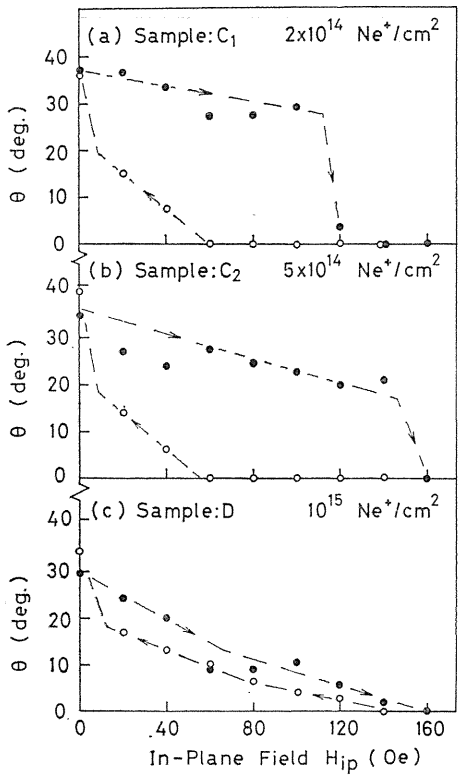

Fig. 3. The θ versus H_{ip} relation in the variously implanted samples; (a) 2×10^{14}, (b) 5×10^{14} and (c) 10^{15} cm^{-2}.

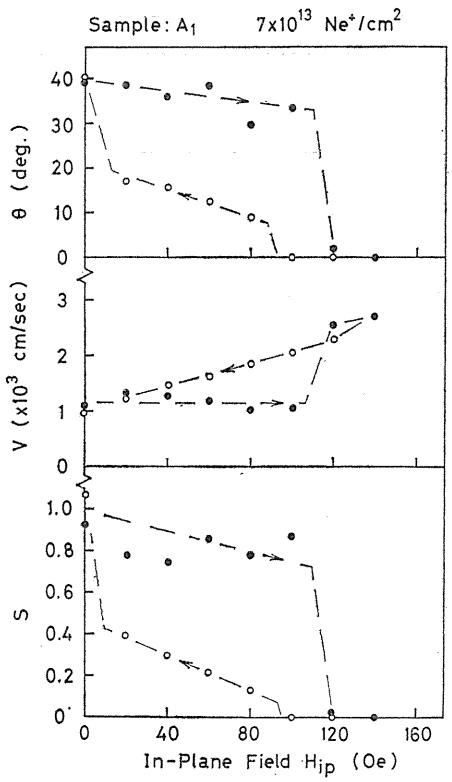

Fig. 4. The dependences of deflection angle θ, translation velocity V and winding number S on in-plane field H_{ip} in the sample A_1.

to a value of about 20 *degrees* but remains at around that value until the transition to the zero deflection angle state at $H_{ip}\simeq120Oe$. During the decrease of H_{ip}, θ remains at almost zero showing no sign of any state transition. Figure 2 (c) shows the θ *vs.* H_{ip} relation in the as-grown sample E. The scatter of the bubble collapse field ΔH_{col} was as large as 37 *Oe*. Therefore, the bubble which was identified to be S=1 from its deflection angle θ of about 35° at $H_{ip}=0$ was again selected as in the case of the 800 Å etched sample B_2. It is noted that the θ *vs.* H_{ip} relation is almost similar to that in the sample B_2 though the transition to the $\theta=0$ state occurs at higher in-plane field of about 160 *Oe*. Again in this case θ does not return to the initial value when H_{ip} is reduced to zero.

Figure 3 shows the effect of the dosage of implanted ions. The sample C_1 in Fig. 3 (a) was implanted to the dosage of 2×10^{14} Ne^+/cm^2 which is about three times as high as that of the reference sample A_1. The θ *vs.* H_{ip} relation is quite similar to that in the sample A_1. The sample C_2 in Fig. 3 (b) was implanted to the dosage of 5×10^{14} cm^{-2}. The θ *vs.* H_{ip} relation is again similar to that in the sample A_1 though θ decreases a little bit at $H_{ip}\simeq20$ *Oe* during the initial increase of H_{ip}. Figure 3 (c) shows the results in the sample D which was implanted to a rather high dosage of $10^{15}cm^{-2}$. With increasing H_{ip}, θ decreases gradually, being

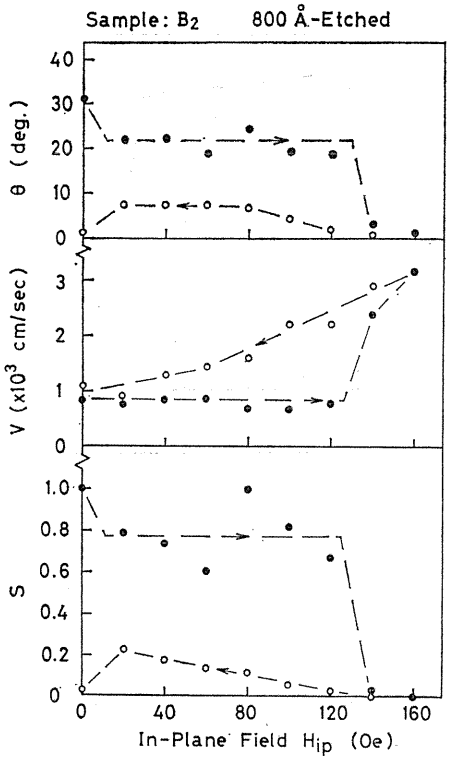

Fig. 5. The dependences of θ, V and S on H_{ip} in the 800 Å etched sample B_2.

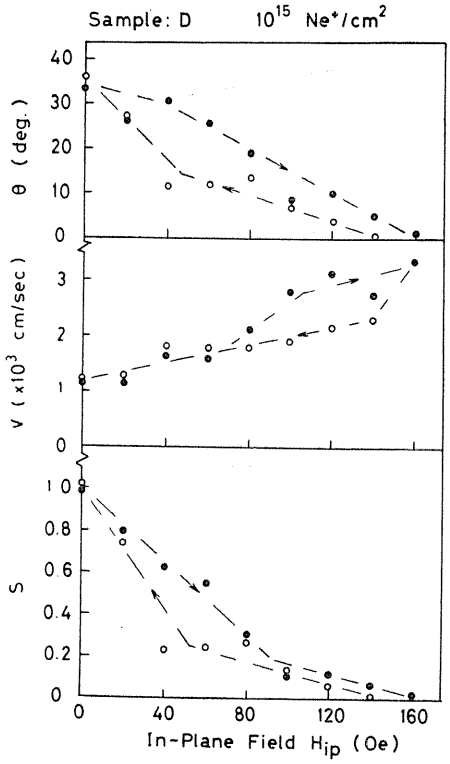

Fig. 6. The dependences of θ, V and S on H_{ip} in the 10^{15} cm^{-2} dosed sample D.

zero at $H_{ip} \simeq 160$ *Oe*. Then with decreasing H_{ip}, θ increases again gradually, returning to the initial value at $H_{ip}=0$. It is noted that any clear transition as seen in the reference sample A_1 is not observed in the sample D. It was also found that there existed the points where the smooth bubble motion was impeded. The scatter of the bubble collapse field ΔH_{col} was as little as 0.7 *Oe*.

In order to calculate the bubble winding number S from eq. (1), the value of the bubble translation velocity V has to be measured in addition to that of θ shown in Figs. 1 ~ 3. Here, the translation velocity V is calculated by $\Delta x/T$, where Δx is the translation distance per pulse and T is the pulse duration. In Figs. 4 ~ 6 are shown the dependences of θ, V and S on H_{ip} in three kinds of typical samples: the reference sample A_1, the 800 Å etched sample B_2 and the 10^{15} Ne^+/cm^2 dosed sample D. In calculating S from eq. (1), the initial bubble state at $H_{ip}=0$ is assumed to be $S=1$ because the value of γ is not available. When $\theta=0$, the bubble state can be, of course, identified to be $S=0$ from eq. (1) regardless of the values of V and other parameters.

Here it should be noted that the simultaneous measurement of both θ and V was rather difficult in the present experimental setup since the angle θ and the distance Δx had to be measured using two kinds of eye-pieces simultaneously as

mentioned in 2. Therefore, the winding numbesr S calculated from eq. (1) using these meaured values of θ and V might include rather large error.

Figure 4 shows the dependence of θ, V and S on H_{ip} in the reference sample A_1. Both V and θ remain almost constant until the first transition at $H_{ip}\simeq 120$ *Oe*. Together with the transition to $\theta=0$, V abruptly increases. Then with decreasing H_{ip}, V decreases almost linearly while θ increases stepwise. The value of S abruptly decreases from $S=0.8$ to $S=0$ at $H_{ip}\simeq 120$ *Oe*, and jumps to $S\simeq 0.1$ when H_{ip} is decreased to about 80 *Oe* and then increases gradually until the final jump from $S\simeq 0.5$ to $S\simeq 1$ at $H_{ip}\simeq 0$.

Figure 5 shows the dependences of θ, V and S on H_{ip} in the 800 $\mathring{A}$ etched sample B_2. As in the case shown in Fig. 2 (b) the bubble with the initial state of $S=1$ was selected. The behavior of θ, V and S with increasing H_{ip} are similar to those in the sample A_1. With decreasing H_{ip}, V decreases almost linearly in the same manner as that of the sample A_1 while θ remains at almost zero and does not return to the initial value at $H_{ip}=0$.

Figure 6 shows the results in the sample D dosed to $10^{15} cm^{-2}$. With increasing and then decreasing H_{ip}, V increases and then decreases almost linearly, though slightly stepwise. Both θ and S behave almost linearly, too.

4. Consideration

4. 1. Magnetic properties of ion-implanted surface layers

By ion-implantation the lattice constant d in the film surface layer is increased by a small amount Δd in the direction perpendicular to the film plane, *i. e.* [111] direction in the samples used here. The strain $\Delta d/d$ induces the magnetic anisotropy through magneto-strictive effect. The induced anisotropy constant K_s is given as follows:

$$K_s=3\lambda_{111}\sigma/2=(3/2)[E/(1-\nu)](\Delta d/d)\lambda_{111}, \tag{2}$$

where λ_{111} is the magnetostriction constant in the [111] direction, σ the compressive stress defined by $[E/(1-\nu)]$ $(\Delta d/d)$, E Young's modulus and ν Poisson's ratio, respectively. Therefore, the effective magnetic anisotropy constant K_{eff} of the ion-implanted layer is expressed as

$$K_{eff}=K_u+K_s=K_u+(3/2)[E/(1-\nu)](\Delta d/d)\lambda_{111}, \tag{3}$$

Where K_u is the uniaxial anisotropy constant of the as-grown film. In the garnet films of $(YEuYbCa)_3(FeGe)_5O_{12}$, λ_{111}, E, ν and K_u are estimated to be -1.4×10^{-6}, $\sim 2\times 10^{12}$ *dyne/cm*^{2}, ~ 0.3 and $\sim 1.3\times 10^4$ *erg/cm*^{3}, respectively[11]. Therefore, the strain $(\Delta d/d)$ larger than 0.002 makes K_{eff} to be negative, laying the magnetic easy direction in the film plane.

The profile of the lattice strain $(\Delta d/d)$ and therefore the effective magnetic anisotropy constant K_{eff} produced by ion-implantation were qualitatively investigated by Engemann *et al*[10]. They utilized the fact that the chemical etching rate is remarkably dependent on the implantation-induced damage. However, the relation between the etching rate and the damage is not yet understood quantitatively. The

damage profile produced by Ne^+ ions has generally the form of Gaussian distribution. The position of the maximum damage, R_p, becomes deeper with increasing the ion energy as schematically shown in Fig. 7. The damage, of course, becomes larger with increasing the dosage. Although a certain amount of strain and hence damage is required to produce the planar magnetization layer, the damage exceeding the upper limit of the "*allowed damage band*" produces the magnetically inactive layer. The reason for this may be that the micro-ferrimagnetic-domains produced by the over-damage could be randomly distributed, causing the average magnetization of the implanted layer to be effectively zero[11]. The qualitative dependence of the thickness of magntically active and inactive layers on the implantation dosage is schematically shown in Fig. 8.

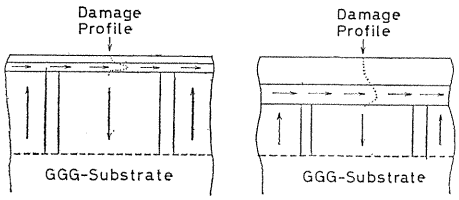

Fig. 7. Model of burried capping layer with an easy direction of magnetization parallel to the film plane. (a) Low implantation energy and (b) high implantation energy. (After Engemann *et al.*[10])

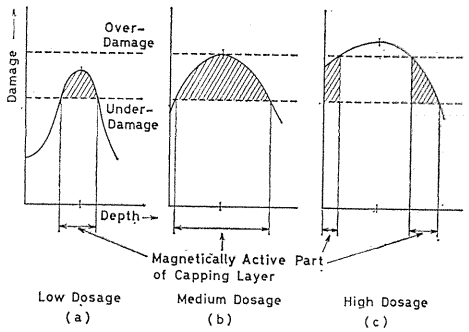

Fig. 8. Qualitative dependence of the magnetically active capping layer thickness on the implantation dosage. With increasing dosage, the magnetically active part of the capping layer becomes larger (a) → (b), and then decreases again (c). The implantation energy is kept constant. (After Engemann *et al.*[10])

Komenou *et al.* recently investigated the crystalline and magnetic properties of ion-implanted surface layer in detail[11]. They studied the crystalline properties (*i. e.* damage profile) by means of the double-crystal X-ray-diffraction method and the magnetic properties by measuring the change of normal-bubble collapse field from that in the as-grown film, respectively, with etching the ion-implanted layers successively. Their samples were prepared in the same runs of LPE and implanted at the same ion energy of 100 *keV* as those used here. Therefore, their results may be compared with the present ones even quantitatively. The relevant results of theirs are shown in Fig. 9. In the case of the dosage of 7×10^{13} cm^{-2} which is the same as that of the reference sample A_1, all the implanted layer is magnetically active and has a planar magnetic anisotropy. In the case of 2×10^{14} cm^{-2} dosage as in the sample C_1, the magnetically inactive region appears in the middle of the implanted layer. In the case of 10^{15} cm^{-2} as in the sample D, a relatively thick surface layer becomes magnetically inactive and only a thin bottom part of the implanted layer functions as the planar magnetization layer.

The planar domains in the ion-implanted surface layer, closure domains, have been observed by Bitter pattern method using "*Ferrofluid*"[8]. Uchishiba *et al.* observed closure domain patterns and investigated the effect of H_{ip} on bubble collapse field H_{col} in ion-implanted films prepared in the same runs as those used here[12]. They found that the threshold value of H_{ip} at which closure domains disappear is strongly dependent on the orientation of H_{ip} with respect to crystallographic axes of the film. As closure domains raise the bubble collapse field ("*flux-keeper effect*"), the existance of closure domains can be detected from the variation of H_{col} associating with the rotation of H_{ip} in the film plane, δH_{col}. They investigated δH_{col} as a function of the Ne^+ ion dosage and found that δH_{col} and therefore a closure domain appear in the range of dosage between 3.5×10^{13} and 3.5×10^{14} cm^{-2}, having a peak at $\sim10^{14}$ cm^{-2}. As discussed later, however, these results do not mean that the effect of ion-implantation is not seen in the films implanted either less than 3.5×10^{13} or more than 3.5×10^{14} cm^{-2}.

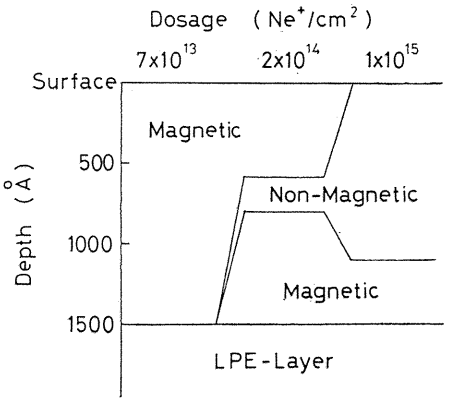

Fig. 9. The magnetic properties of surface layers of $(YEuYbCa)_3(GeFe)_5O_{12}$ films implanted to various dosages with 100 *keV* Ne^+ ions. (Afrte Komenou *et al.*[11])

4. 2. Model for bubble state transition in ion-implanted films

Beaulieu *et al.* investigated the relationship between the wall states of translating bubbles in ion-implanted garnet films and an in-plane field H_{ip} by means of the "*deflectometer*" method[17]. The deflectometer was made of a lot of parallel conductors deposited on the film surface. Bubbles were propagated back and forth over a distance of ~200 μm by passing pulse currents through the pair of conductors sequentially. Thus, the deflectometer provides very high angular resolution ($\sim0.7°$) at the expense of the nonuniformity of drive field and therefore translation velocity. The relation between bubble deflection angle θ and an in-plane field H_{ip} reported

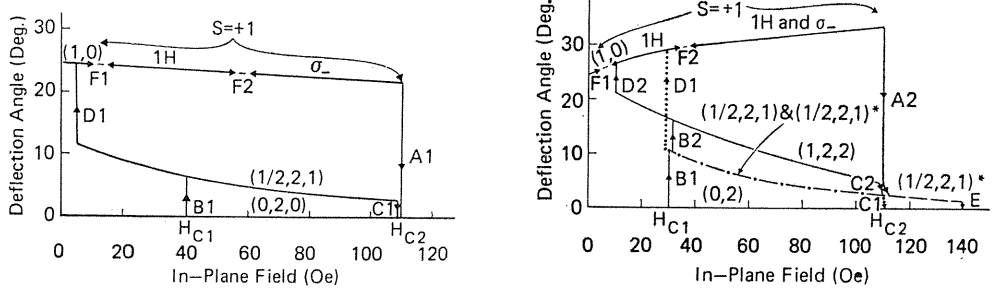

Fig. 10. The θ versus H_{ip} relation reported by Beaulieu *et al.*[17] H_{ip} is applied parallel and perpendicular to ∇H in (a) and (b), respectively.

by them is shown in Fig. 10, where H_{ip} is applied either parallel or perpendicular to the pulsed gradient field ∇H. In order to describe the detail of bubble wall staructure, they employed the three digit notation (S, L, P) where S is the bubble revolution number, L the number of vertical Bloch lines and P the number of Bloch points, respectively. As seen from Figs. 10 (a) and (b), they found nine different state transitions A_1~E at which the deflection angle changes abruptly. In order to interpret these state transitions they found it necessary to "*invoke*" four $S=1$ states (unichiral $S=1$, $1H$ having two horizontal Bloch loops, σ (1, 2, 0), and (1, 2, 2)), two $S=1/2$ states ((1/2, 2, 1) and (1/2, 2, 1)*) and one $S=0$ state, (0, 2, 0). Since most of the experimental results shown in 3 are in the case of $H_{ip}//\nabla H$ and the transition mechanism is simpler than that in the case of $H_{ip} \perp \nabla H$, we show the outline of their model for the wall state transitions in the case of $H_{ip}//\nabla H$ below.

Only unichiral S=1 bubble (1, 0, 0) exists stably in adequately ion-implanted films under zero in-plane field (Fig. 11(a)). During the translation under in-plane field, two horizontal Bloch loop (*HBL*'s) nucleate in the wall segment where the nucleation threshold of *HBL* is lower than other parts because the magnetization is opposite to H_{ip} (Fig. 11(b)). Since the capping layer, due to a large exchange repulsion, resists punch-through of *HBL* at the top surface, the *HBL* generated at the top surface may propagate down and finally punch-through at the lower surface (Fig. 11 (c)). With increasing H_{ip} the *HBL* generated at the lower surface is pushed down by the punched-through *HBL* to shrink and finally disappear. The resultant wall state is σ (1, 2, 0) (Fig. 11 (d)). When H_{ip} is further incresed up to the critical value H_{c2} (Fig. 10), the implanted layer is completely magnetized along the direction of H_{ip} and the closure domain disappears ("*cap switching*"). At the same time, the Bloch point (*BP*) is injected into the *VBL* underlying the closure domain (Fig. 11(e)). The injected *BP* is propagated down by the magnetostatic force caused by H_{ip}, reversing the *VBL* polarity to produce $S=0$ bubble, (0, 2, 0) (Fig. 11 (f)). When H_{ip} is decreased to the critical value H_{c1}, a closure domain again appears and consequently a *BP* is injected into the underlying *VBL* (Fig. 12 (b)). With decreasing H_{ip}, the injected *BP* is propagated down to the midpoint of the *VBL* increasing the revolution number S to 1/2 gradually. The transition D_1 is caused by the gyrocoupling force F_g exerted on *VBL*'s. Though the total $\vec{F}_g$ is zero on the *VBL* with a *BP* at the midpoint, the *VBL* without *BP* is circulated around the bubble wall by $\vec{F}_g$ (Fig.

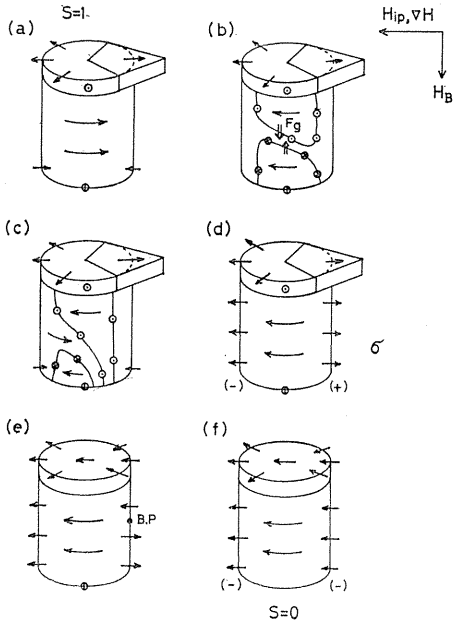

Fig. 11. Schematic representation of bubble state transitions with increasing H_{ip} proposed by Beaulieu *et al.*[17] The detail of process is summarized in the text.

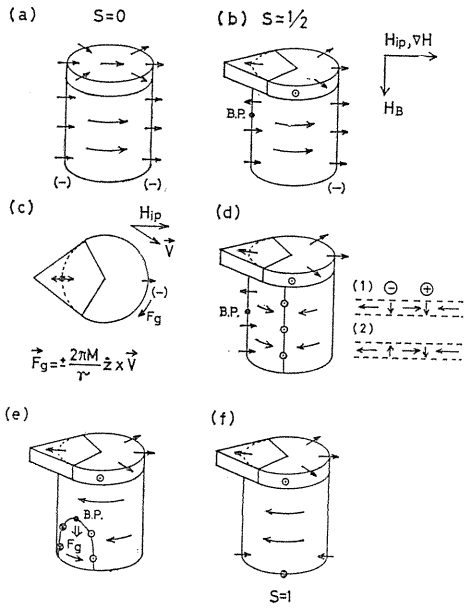

Fig. 12. Schematic representation of bubble state trasitions with decreasing H_{ip}.[17]

12 (c)). The upper half of both *VBL*'s attracts each other by the magnetostatic force, as shown in the inset of Fig. 12 (d), to collide and unwind. The resulted Bloch loop shrinks away with decreasing H_{ip} (Fig. 12 (e)). Thus, the wall state returns its initial unichiral $S=1$, (1, 0, 0) (Fig. 12). In the case of $H_{ip} \perp \nabla H$, the transition mechanism is basically similar to that of $H_{ip} // \nabla H$ though more complicated.

Thus, it should be noted that most of the wall state transitions detected by the abrupt change of bubble deflection angle are associated with the nucleation or anihilation of a closure domains in this model. That is, the behavior of a closure domain plays the "*key*" role in this model.

4. 3. Effects of surface etching and ion dosage on state transitions

Now we consider the experimental results shown in 3. based on the relevant works summarized in the last subsections.

First of all, it is noted that the relationship between the bubble deflection angle θ and the in-plane field H_{ip} in the reference sample A_1 shown in Fig. 1 is quite similar to that reported by Beaulieu *et al.* shown in Fig. 10. As mentioned in *4. 1.*, whole of the implanted layer ranging to the depth of 1500 Å is the planar magnetization layer and the closure domains associating with the underlying bubbles are observed in the samples implanted to a dosage of 7×10^{13} cm^{-2}. Therefore, the bubble state transition model proposed by Beaulieu *et al.*, where the existance of a closure domain is essential as summarized in *4. 2.*, might be adequate for the reference sample A_1.

The effect of the removal of the ion-implanted layer is shown in Fig. 2. The θ *vs.* H_{ip} relation in the sample A_2, the surface of which was etched by 480 Å, shown in Fig. 2 (a) is quite similar to that in the sample A_1, showing no significant influence of the removal of the surface layer. However, the θ *vs.* H_{ip} relation in the sample B_2, the surface layer of which was etched by 800 Å, shown in Fig. 2(b) is quite different from that in the sample A_1. The transition from $S=1$ to $S=0$ is observed, but the bubble does not return to the initial state after reducing H_{ip} to zero. In addition, the scatter of the collapse field ΔH_{col} among lots of bubbles, which is considered to be another measure indicating the effectiveness of ion-implantation, was as large as 12 *Oe*. These results suggest that the most effective planar magnetization layer exists in the layer ranging from 500 to 800 Å deep in the samples implanted to a standard dosage of 7×10^{13} cm^{-2} at 100*keV*, though the magnetically active layer ranged to a depth of 1500 Å as shown in Fig. 9.

It is noted that the transition from $S=1$ to $S=0$ is observed in the 800 *A*-etched sample B_2 and even in the as-grown sample E. These results suggest that the

transition from $S=1$ to $S=0$ does not require the existance and then anihilation of the closure domain as in the model proposed by Beaulieu *et al.* As mentioned in *4. 2.*, Obokata *et al.* found that the threshold value of H_{ip} at which the closure domain disappeared depended strongly on the orientation of H_{ip} with respect to the crystallographic axis of a film, *e.g.*, ranging from 35 to 150 *Oe* in the film implanted to a dosage of 2×10^{14} cm^{-2} at 100 *keV*. To the contrary, Beaulieu *et al.* reported that the threshold value of H_{ip} at which the transition from $S=1$ to $S=0$ occured was almost independent of the orientation of H_{ip}. These facts seem to support the above consideration that the transition from $S=1$ to $S=0$ does not necessarily require the existance and the anihilation of the closure domain. Of couse, this does not mean that the closure domain does not play any role in this transition.

On the other hand, the state transition from $S=0$ to $S=1/2$ during the decrease of H_{ip} was not observed either in the 800 $\mathring{A}$-etched sample B_2 or in the as-grown sample E. These results seem to suggest that the transition from $S=0$ to $S=1/2$ do always require the nucelation of the closure domain as in the model proposed by Beaulieu *et al.* However, further discussion on this transition will be given later in conjunction with the effect of an implantation dosage.

Now we consider the effect of an ion dosage shown in Fig. 3. The θ *vs.* H_{ip} relation in the sample C_1 implanted to a dosage of 2×10^{14} cm^{-2} is quite similar to that in the sample A_1. The effect of a thin non-magnetic layer existing in the middle of the implanted layer (see Fig. 9) seems to be little. The θ *vs.* H_{ip} relation in the sample C_2 implanted to a dosage of 5×10^{14} cm^{-2} is again similar to that in the sample A_1, though a little decrease in θ at H_{ip} 20 *Oe* during the initial increase of H_{ip} is observed. This initial decrease of θ might reflect the effect of the rather thick non-magnetic layer existing in the middle of the implanted layer and/or the effect of the absence of closure domains. The θ *vs.* H_{ip} relation in the sample D implanted to a dosage of 10^{15} cm^{-2} is quite different from that in the reference sample A_1. No abrupt transition is observed with increasing and decreasing H_{ip}. Although the effective thickness of the planar magnetization layer is reduced in this sample as shown in Fig. 9, the bubble state at $H_{ip}=0$ is still determined uniquely. In addition, the scatter of the bubble collapse field, ΔH_{col}, is as small as 0.7*Oe*. Considering the fact that the closure domain was not observed in higher dosage samples, the model proposed by Beaulieu *et al.* may not be applicable to the samples C_2 and D.

Obokata *et al.* found that the θ *vs.* H_{ip} relation depended on the implantation condition[19]. The θ *vs.* H_{ip} relation in the sample having closure domains depended on the orientaion of H_{ip} while that in the sample without closure domain did not. They concluded that the transiton from $S=0$ to $S=1/2$ might be triggered by the injection of a *BP* into a *VBL* due to the stray field of the bubble when the sample had no closure domain. The θ *vs.* H_{ip} relation in the sample C_2 without closure domain mihgt be explained by the model proposed by Beaulieu *et al.* in conjunction with this *BP* injection process.

The θ *vs.* H_{ip} relation in the sample D is rather similar to that reported by Josephs *et al.*[16] They proposed the wall structure including two *VBL*'s each containing a *BP* as shown in Fig. 13. When H_{ip} is not applied, both *BP*'s are positioned at the midplane of the film and the bubble wall is made up of two types of σ bubbles, $(1, 2, 0)_{\pm}$, separated at the midplane of the film. With increasing H_{ip}, the *BP*'s move apart reducing the value of S from 1 to 0, the final state being (0, 2, 0). Using this model, the θ *vs.* H_{ip} relation in the sample D seems to be

explained satisfactorily. However, there are still problems such as how the rather complicated $S=1$ wall structure at $H_{ip}=0$ is realized.

The *BP* injection into the *VBL* due to the bubble stray field takes place in the heavily implanted samples C_2 and probably D, but the injection does not take place in the 800 Å-etched sample B_2 and the as-grown sample E. This fact may lead us to the conclusion that the *BP* injection due to the stray field also require the existance of some planar magnetization layer.

In the sample D, it was also found that there existed some local points where the bubble translation coercivity is so high that the smooth translation is impeded. These points might be produced by the implantation damage exceeding the limit of the elastic deformation of the film locally.

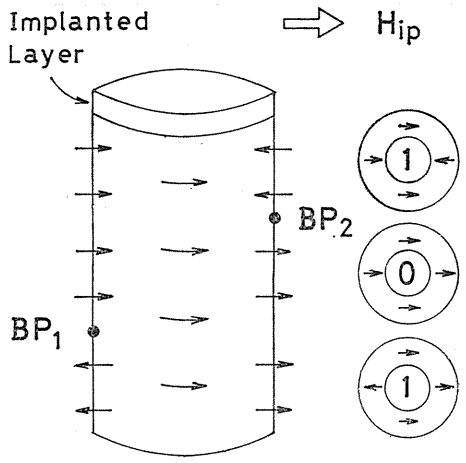

Fig. 13. Model of the bubble wall having two Bloch lines each containing one Bloch point.[16] The bubble sections viewed from the top of the bubble correspond to three kinds of wall structures separated by two *BP*'s. The *S* numbers are shown at the center of each bubble section.

Finally we consider the dependences of θ, V and S on H_{ip}. Comparing the dependence of S on H_{ip} with that of θ on H_{ip} in the reference sample A_1, it is seen that the bubble deflection angle θ is a very good measure of the bubble winding number S. Both of the dependence of S on H_{ip} and that of θ on H_{ip} in the 800 Å-etched sample B_2 are quite different from those in the sample A_1. However, the dependence of V on H_{ip} is quite similar to each other. In this sample B_2, θ is a good measure of S. The V *vs.* H_{ip} relation as well as the θ *vs.* H_{ip} relation is quite peculiar in the heaviest dosed sample D. Even in this sample, however, θ is a good measure of S. Thus, θ is a good measure of S in any case. This fact suggests that a value of S can be deduced from only a value of θ independent of V, which is the fundamental hypothesis assumed in the "*deflectometer*" method.

The effect of H_{ip} on V had been discussed in detail previously.[21]

5. Conclusion

The effect of the ion-implanted surface layer on the relationship between the bubble deflection angle θ and the in-plane field H_{ip} was investigated using the samples either etched a part of the implanted layer or implanted to various dosages.

In the samples implanted to a dosage of 7×10^{13} Ne^+/cm^2 at $100keV$, where a closure domain accompanied by the underlying bubble is clearly observed, the removal of the implanted surface layer by 480 Å does not affect the θ *vs.* H_{ip} relation significantly but the removal of further 300 Å changes it substantially.

In the samples implanted to as high dosage as 5×10^{14} cm^{-2}, where the closure

domain is no more observed, the θ *vs.* H_{ip} relation does not differ substantially from that in the reference sample implanted to a dosage of 7×10^{13} cm^{-2}. However, in the sample implanted to higher dosage of 10^{15} cm^{-2} θ varies with increasing and then decreasing H_{ip} gradually rather than abruptly as in the reference sample.

These experimental results were interpreted based on the previous works on the magnetic properties of the implanted surface layers and the bubble state transitions. The θ *vs.* H_{ip} relations resembling to that observed in the reference sample seem to be explained by the bubble state transition model proposed by Beaulieu *et al.*, if necessary, in conjunction with the Bloch point injection mechanism into a vertical Bloch line due to the bubble stray field proposed by Obokata *et al.* The θ *vs.* H_{ip} relation in the sample implanted to the highest dosage of 10^{15} cm^{-2} seems to require further theoretical investigations.

A bubble winding or revolution number S was calculated from the theoretical equation using the values of both the bubble deflection angle θ and the bubble translation velocity V measured simultaneously. It was found that the S *vs.* H_{ip} relation was quite similar to the θ *vs.* H_{ip} relation in any case, and confirmed that a bubble state characterized by the value of S could be deduced from only the value of θ.

Acknowledgements

This work was carried out by one of the authors (S. S.) at Fujitsu Laboratories Ltd., Kawasaki, Japan, by courtesy of Mr. K. Yamagishi, a vice-president, and Mr. S. Orihara, a manager of bubble device section. Thanks are due to them and other members of bubble section at Fujitsu Laboratories Ltd. The authors also express their appreciation to Dr. S. Tsunashima and other members of Uchiyama Laboratory for their valuable discussions.

References

1) R. Wolfe and J. C. North: Bell System Tech. J., **51** (1972) 1436.
2) T. Hsu: AIP Conf. Proc., No. 24 (1974) 624.
3) O. Voegeli, B. A. Calhoun, L. L. Rosier and J. C. Slonczewski : AIP Conf. Proc., No. 24 (1974) 617.
4) G. S. Almasi, E. A. Giess, R. J. Hendel, G. E. Keefe, Y. S. Lin and M. Slusarczuk : AIP Conf. Proc., No. 24 (1974) 630.
5) Y. S. Lin, G. S. Almasi and G. E. Keefe : IEEE Trans. Magn., **MAG-13** (1977) 1774.
6) Y. S. Lin, G. S. Almasi and G. E. Keefe : J. Appl. Phys., **48** (1977) 5201.
7) R. Wolfe, J. C. North and Y. P. Lai : Appl. Phys. Lett., **22** (1973) 683.
8) R. Wolfe and J. C. North : Appl. Phys. Lett, **25** (1974) 122.
9) H. Jouve, J. P. Gailliard and J. Piaguet : IEEE Trans. Magn., **MAG-11** (1975) 1082.
10) J. Engemann and T. Hsu : Appl. Phys. Lett., **30** (1977) 125.
11) K. Komenou, I. Hirai, K. Asama and M. Sakai : J. Appl. Phys., **49** (1978) 5816.
12) H. Uchishiba, T. Obokata and K. Asama: J. Appl. Phys., **48** (1977) 2604.
13) J. C. Slonczewski, A. P. Malozemoff and O. Voegeli : AIP Conf. Proc., No. 10 (1972) 458.
14) D. C. Bullock: AIP Conf. Proc., No. 18 (1973) 232.

15) R. Hasegawa: AIP Conf. Proc., No. 24 (1974) 615.
16) R. M. Josephs, B. F. Stein ane W. R. Bekebrede : AIP Conf. Proc., No. 29 (1975) 65.
17) T. J. Beaulieu, B. R. Brown, B. A. Calhoun, T. Hsu and A. P. Malozemoff : AIP Conf. Proc., No. 34 (1976) 138.
18) T. Obokata, K. Yamaguchi and K. Asama : AIP conf. Proc., No. 29 (1976) 74.
19) T. Obokata, H. Uchishiba and K. Asama : IEEE Trans. Magn., **MAG-13** (1977) 1181.
20) G. P. Vella-Coleiro and W. J. Tabor : Appl. Phys. Lett., **21** (1972) 7.
21) S. Shiomi, A. Ikai, Y. Sawada, S. Iwata, S. Uchiyama and T. Fujii : Memoirs of the Faculty of Engineering, Nagoya Univrsity, **31**, No. 2. November (1979) 184.